Remote sensing of bark beetle damage in urban forests at individual tree level using a novel hyperspectral camera from UAV and aircraft

Näsi, Roope

2018-03

Näsi , R , Honkavaara , E , Blomqvist , M , Lyytikäinen-Saarenmaa , P M E , Hakala , T , Viljanen , N , Kantola , T A & Holopainen , M E 2018 , ' Remote sensing of bark beetle damage in urban forests at individual tree level using a novel hyperspectral camera from UAV and aircraft ' , Urban Forestry & Urban Greening , vol. 30 , UFUG 26057 , pp. 72-83 . https://doi.org/10.1016/j.u

http://hdl.handle.net/10138/234793
https://doi.org/10.1016/j.ufug.2018.01.010

Urban Forestry & Urban Greening 30 (2018) 72–83

Contents lists available at ScienceDirect

Urban Forestry & Urban Greening

journal homepage: www.elsevier.com/locate/ufug

Remote sensing of bark beetle damage in urban forests at individual tree level using a novel hyperspectral camera from UAV and aircraft

Roope Näsi[a,*], Eija Honkavaara[a], Minna Blomqvist[b], Päivi Lyytikäinen-Saarenmaa[b], Teemu Hakala[a], Niko Viljanen[a], Tuula Kantola[c], Markus Holopainen[b]

[a] Department of Remote Sensing and Photogrammetry, Finnish Geospatial Research Institute, Geodeetinrinne 2, 02430 Masala, Finland
[b] Department of Forest Sciences, P.O.B. 27, FI-00014, University of Helsinki, Finland
[c] Knowledge Engineering Laboratory, Department of Entomology, Texas A&M University 2475 TAMU College Station, Texas, 77843-2475, USA

ARTICLE INFO

Keywords:
Classification
Forest health
Insect damage
Mapping
Photogrammetry
Spectrometry

ABSTRACT

Climate-related extended outbreaks and range shifts of destructive bark beetle species pose a serious threat to urban boreal forests in North America and Fennoscandia. Recent developments in low-cost remote sensing technologies offer an attractive means for early detection and management of environmental change. They are of great interest to the actors responsible for monitoring and managing forest health. The objective of this investigation was to develop, assess, and compare automated remote sensing procedures based on novel, low-cost hyperspectral imaging technology for the identification of bark beetle infestations at the individual tree level in urban forests. A hyperspectral camera based on a tunable Fabry-Pérot interferometer was operated from a small, unmanned airborne vehicle (UAV) platform and a small Cessna-type aircraft platform. This study compared aspects of using UAV datasets with a spatial extent of a few hectares (ha) and a ground sample distance (GSD) of 10–12 cm to the aircraft data covering areas of several km^2 and having a GSD of 50 cm. An empirical assessment of the automated identification of mature Norway spruce (*Picea abies* L. Karst.) trees suffering from infestation (representing different colonization phases) by the European spruce bark beetle (*Ips typographus* L.) was carried out in the urban forests of Lahti, a city in southern Finland. Individual spruces were classified as healthy, infested, or dead. For the entire test area, the best aircraft data results for overall accuracy were 79% (Cohen's kappa: 0.54) when using three crown color classes (green as healthy, yellow as infested, and gray as dead). For two color classes (healthy, dead) in the same area, the best overall accuracy was 93% (kappa: 0.77). The finer resolution UAV dataset provided better results, with an overall accuracy of 81% (kappa: 0.70), compared to the aircraft results of 73% (kappa: 0.56) in a smaller sub-area. The results showed that novel, low-cost remote sensing technologies based on individual tree analysis and calibrated remote sensing imagery offer great potential for affordable and timely assessments of the health condition of vulnerable urban forests.

1. Introduction

Drivers of global climate change may affect urban woodlands more rapidly than natural forest ecosystems. Stressors of urban forest ecosystems include alterations in forest soils and to the diversity and composition of the urban ecosystem, as well as higher temperatures and increasing carbon dioxide content (Alvey, 2006; Tubby and Webber, 2010). Therefore, urban forests face many threats (e.g., insect pests and diseases) that can affect the overall health of the forest and related benefits. Insect pests can cause extensive ecological damage and economic costs to urban woodlands, either through the direct or indirect effects of climate change on insects (Lyytikäinen-Saarenmaa et al., 2006; Aukema et al., 2011). Proactive management practices and a focused novel monitoring methodology are needed to protect urban forests against the threats posed by insect pests.

One of the most significant threats to boreal forests is climate-related extended outbreaks and range shifts of the destructive bark beetle species (e.g., Safranyik et al., 2010; Kärvemo et al., 2016; Ghimire et al., 2016). In Finland, the European spruce bark beetle (*Ips typographus* L.) (Coleoptera: Curculionidae) has been undergoing a poleward range shift as a damage-causing agent due to elevated summer temperatures and early springs since 2010 (P. Lyytikäinen-Saarenmaa,

* Corresponding author.
E-mail addresses: roope.nasi@nls.fi (R. Näsi), eija.honkavaara@nls.fi (E. Honkavaara), minna.blomqvist@helsinki.fi (M. Blomqvist), paivi.lyytikainen-saarenmaa@helsinki.fi (P. Lyytikäinen-Saarenmaa), teemu.hakala@nls.fi (T. Hakala), niko.viljanen@nls.fi (N. Viljanen), tuulak@tamu.edu (T. Kantola), markus.holopainen@helsinki.fi (M. Holopainen).

https://doi.org/10.1016/j.ufug.2018.01.010
Received 21 December 2016; Received in revised form 14 December 2017; Accepted 9 January 2018
Available online 12 January 2018

unpublished data). Climatic anomalies, such as more frequent and intensive heavy winds and prolonged periods with low amounts of precipitation, have resulted in a multitude of windthrows and stressed Norway spruces (*Picea abies* Karst.). These trees provide optimal breeding material for bark beetles, facilitating the elevating population levels. Consequently, expansive damage spots with visible crown symptoms are present in southern and central parts of Finland, threatening the sustainability of mature Norway spruce stands. It is important to identify colonized trees at an early phase and initiate management operations to protect healthy stands. Bark beetles can cause dramatic, irreversible alterations both in natural and urban forest environments. Especially in urban forests, it is of great importance to maintain safe pathways and aesthetic values, because forests in such areas enjoy high levels of recreational use by citizens.

The vision for the future of precision forestry includes storing forest information at the individual tree level in geographical information systems (GIS) (Holopainen et al., 2014). Such systems are already available or currently being created for urban areas in many Finnish cities (Tanhuanpää et al., 2014). The database should include information about tree locations and various attributes, such as species, height, and stem volume. Several efficient remote sensing technologies are now available for providing this information, including airborne-, mobile-, and terrestrial laser scanning (ALS, TLS, MLS) and stereo imagery (White et al., 2016). Information on tree health and quality are more demanding to measure and typically obtained using multi- or hyperspectral technologies or field measurements (Hall et al., 2016; Senf et al., 2017). Furthermore, since these parameters can change rapidly, the methods affordable for frequent, annual monitoring are of great interest, particularly in small-scale urban woodlands.

Recent developments in multi- and hyperspectral remote sensing technologies are providing new solutions for vegetation health mapping (Torresan et al., 2017). In particular, developments in miniaturized sensor technologies have facilitated the production of low-cost and lightweight multispectral and hyperspectral cameras that enable accurate remote sensing measurements. Several light-weight hyperspectral sensors have already been developed (Aasen et al., 2015). One type of camera is based on the Fabry-Pérot interferometer (FPI) technique (Mäkynen et al., 2011; Honkavaara et al., 2013; Oliveira et al., 2016) and was used in this study. This technology has already shown potential in close-range environmental mapping with unmanned aerial vehicles (UAVs), such as monitoring the health of vegetation (Näsi et al., 2015; Moriya et al., 2017) and classifying tree species (Nevalainen et al., 2017). Important advantages of the FPI technology in comparison to the conventionally used pushbroom technology include the possibility to collect image blocks with stereoscopic multiple object views; the important consequences of which include more extensive datasets, a simplified data processing phase, and reduced costs to the overall system (Honkavaara et al., 2013).

Lightweight, low-cost hyperspectral sensors combined with cost-efficient platforms, such as single-engine manned aircraft or UAVs, offer a tool for the timely monitoring and identification of insect-induced alterations in forest vegetation (Lehmann et al., 2015). Both platforms have their pros and cons with respect to environmental remote sensing tasks. UAVs typically have to be operated in the visible line-of-sight at low flight altitudes due to legislative issues. As a result of these requirements, multicopters are the most useful vehicles for such tasks because they can be used for repeated high-resolution mapping tasks within small areas (Siebert and Teizer, 2014). Small aircrafts are efficient in covering larger areas; on the other hand, their initialization cost is more expensive and they produce lower spatial resolution data than UAVs. The low-cost methods can revolutionize the entire environmental remote sensing process. The conventional high-end hyperspectral sensors are typically expensive and rare, thus obtaining data from these systems can be more difficult and costly. In contrast, these low-cost systems can be owned and operated locally by small companies, thus making it easier to organize remote sensing campaigns and also multitemporal monitoring acquisitions.

A review by Senf et al. (2017) showed that recent research related to the remote sensing of insect pest damage has focused on conifer bark beetles and defoliators of deciduous trees. Among bark beetles, the mountain pine beetle (Dendroctonus ponderosae Hopkins) in North America and European spruce bark beetle (I. typographus) are the most studied insect pests, especially in the last few years. Satellite images, such as Landsat (Havasová et al., 2015; Foster et al., 2016; Long and Lawrence, 2018), have been the most utilized, whereas hyperspectral sensors have been used only in a few studies (Senf et al., 2017). Näsi et al. (2015) were the first to utilize UAV-based hyperspectral image data for identifying different infestation stages of the bark beetle. Their results showed that different stages (i.e., healthy, infested, and dead trees) could be identified by machine vision technologies based on hyperspectral UAV imaging at the individual tree level; the results for the overall accuracy were 76% when using three color classes (healthy, infested, dead). For two color classes (healthy, dead), the best overall accuracy was 90%. Their conclusions were that survey methodology based on high-resolution hyperspectral imaging will be of great practical value for forest health management, capable for instance of indicating the potential for a bark beetle outbreak at a particular time.

Studies using conventional pushbroom scanning-based hyperspectral sensors from aircraft platforms for the mapping of bark beetle damage using area-based methods have shown promising results. Fassnacht et al. (2014) reported an overall accuracy rate of 76–85% when three health classes of trees and two types of soil were classified. Lausch et al. (2013) were able to classify three health classes with an overall accuracy rate of 69%. Only a minor proportion of studies on bark beetle damage have used high spatial resolution (ground sample distance, GSD $<$ 1 m) data (Senf et al., 2017), which is a prerequisite for individual tree-level approaches. Meddens et al. (2011) and Lausch et al. (2013) have reported that enhancing the spatial resolution of remote sensing images improves the classification results for bark beetle damage. However, in both studies researchers performed their analysis at the area or pixel level as opposed to adopting an individual tree-level-based approach. Recent developments in sensors and UAV technologies are enabling analysis at the individual tree level because many pixels can be obtained from each tree due to the small GSD. However, only a few studies have analyzed pest damage at the individual tree level. For example, Minařík and Langhammer (2016) presented preliminary results using a UAV equipped with a multispectral sensor to map bark beetle damage and Dash et al. (2017) used a multispectral sensor to classify a disease outbreak in mature Pinus radiata D. Don using a UAV as a platform. More information about state-of-the-art remote sensing of forest insect damage can be found in the extensive reviews provided by Hall et al. (2016) and Senf et al. (2017). Furthermore, Lausch et al. (2016, 2017) have presented comprehensive reviews of remote sensing methods used to assess forest health that cover various types of damage, including insect damage, drought, invasive species, air pollution, and land-use changes.

The fundamental motivations for this investigation were to assess whether or not low-cost FPI camera technology can provide useful remote sensing data on the health of spruce trees in urban forests via aircraft or a UAV platform and to compare these two platforms. The same camera was operated using aircraft over an area of several square kilometers as well as a small UAV to identify symptoms in small areas. Accordingly, our main goals were to i) develop and assess a novel, low-cost, miniaturized, hyperspectral remote sensing technology for observing bark beetle infestation at the individual tree level in urban Norway spruce stands, ii) compare automated remote sensing procedures when operated from UAV and aircraft platforms.

The preliminary analyses of the UAV datasets were presented by Näsi et al. (2015). The current work emphasizes the aircraft data analysis and comparison of the UAV and aircraft results as well as production of spruce health maps. This study provides new information about the applicability of novel remote sensing technologies for tree

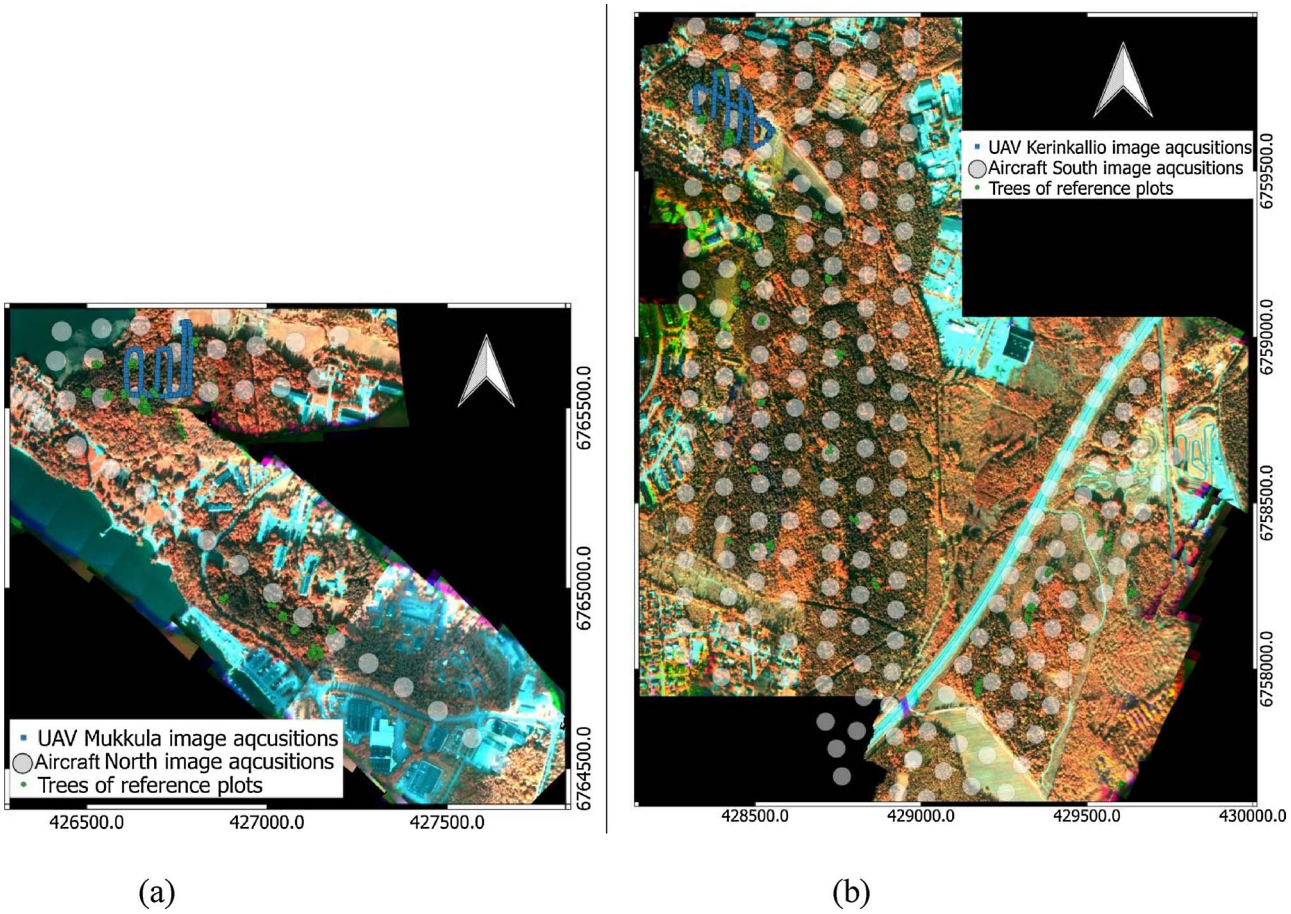

Fig. 1. Flight trajectories and locations of the reference trees in Lahti in the a) north area and b) south area. The background image is a radiometrically corrected reflectance mosaic combination of FPI bands 23, 9 and 1.

assessment in order to support decision-making regarding urban forest management.

2. Materials and methods

2.1. Test area and ground truth

The field work was conducted in urban forests in the city of Lahti, in southern Finland (60°59′N, 25°39′E), in 2013. These urban forests, covering approximately 5000 ha, are dominated by mature Norway spruce stands growing in fertile soils (*Oxalis-Maianthemum, Oxalis-Myrtillus* and *Myrtillus* site types) (Cajander, 1926). The forests are used quite often for recreational purposes by residents throughout the year. Bark beetle (*I. typographus*) has been causing damage, including tree mortality, both in the city area and in adjacent urban woodlands since 2010. This study was part of a larger field campaign carried out in the city of Lahti, aiming to investigate shifts in the population density of *I. typographus* in the city forests.

We had two areas of interest: the "north area," about three km north of the city center, and the "south area," about two km southeast of the city center (Fig. 1). These areas suffered from *I. typographus* infestations, stimulating the need to use UAVs. An aerial color-infrared imagery with 0.5 m spatial resolution (National Land Survey of Finland, Topographic Database 06/2013) was utilized for a preliminary visual detection of spots of dead Norway spruces prior to the field campaign in 2013. Based on this inspection, the locations of the study plots (n = 45) were assigned to the *I. typographus* infestation spots. A total of 48 circular sampling plots (radius = 10 m) were inventoried and assessed within the study areas in 2013. Three of the sampling plots had already been established in 2012 during a pilot study. The center of each plot was located with a Trimble Geo XT GPS device (Trimble Inc., Sunnyvale, CA, USA), having a precision of 0.5 m with differential post-processing. Each individual tree on our plots was located by measuring the azimuth and distance from the center of the sampling plot.

Field inventory and visual assessments of the health of the Norway spruce were conducted in August 2013. Bark beetle-induced symptoms are typically most visible to the human eye late in the growing season. In total, 330 mature Norway spruce trees were included in the analysis. Tree-wise measurements included diameter at breast height (dbh) (cm) for each tree and the tree height (m) from a median tree and every seventh tree throughout the plots (Table 1). In addition to inventorying dead spruces, we assessed crown symptoms of the living spruce trees, both healthy and infested, on the plots. The spruce trees were assessed relative to each other by two experienced observers, who calibrated their eyes prior to the field campaign. The assessed symptoms were crown discoloration and defoliation. These attributes are typical symptoms indicating the infestation status of *I. typographus*. The trees were classified based on the crown color into four classes: green

Table 1
Class-wise number (n) of Norway spruce trees, diameter at breast height (d, cm) and height (h, m) of the sampled trees measured in 2013 (mean = the average, min = minimum, max = maximum and sd = standard deviation of measurements; classes include: healthy such as green, class 1; infested such as yellowish, class 2; and dead such as gray, class 4).

Class	n	d_{mean}	d_{min}	d_{max}	d_{sd}	h_{mean}	h_{min}	h_{max}	h_{sd}
Healthy	246	36.9	25.1	61.0	7.2	30.2	22.1	39.0	3.5
Infested	20	36.4	26.2	48.5	6.0	30.2	26.2	34.8	3.8
Dead	64	37.5	26.0	51.8	7.0	30.7	27.8	34.8	2.5

(healthy, class 1), yellowish (yellow attack, class 2), reddish (red attack, class 3), and gray (dead tree, class 4). Both healthy trees and trees with a potential early infestation stage (green attack) were treated as one class in this study. Reddish crowns (class 3) represented a minor proportion of the current data and were excluded from the analyses. We also eliminated smaller trees (dbh < 25 cm) from the analyses. Such suppressed trees are likely to remain in the shadows of dominant trees and have very low reflectance values. Trees growing at lower canopy cover layers are also more likely to be defoliated by factors other than beetle infestation. Furthermore, *I. typographus* is known to prefer trees with a large dbh (Göthlin et al., 2000), and most likely only a minor proportion of these smaller trees where colonized by the beetle.

The previous study by Näsi et al. (2015) was carried out using UAV-based remote sensing datasets, collected in small areas in "Mukkula" (part of the north area) and "Kerinkallio" (part of the south area). These subareas included a total of 78 reference trees and are referred to as set 1 in the analysis (Fig. 1). The reference trees outside the UAV study areas form set 2 of the reference trees.

2.2. Remote sensing materials

The aircraft campaign using a Cessna 172 OH-CAH (operated by Lentokuva Vallas Oy) was carried out on September 13, 2013 (Table 2). The FPI hyperspectral camera (Mäkynen et al., 2011) was employed as an imaging sensor. The areas covered were 1 km^2 (north area) and 3.5 km^2 (south area). Images were collected using a flying altitude of 500 m (Table 2). In the resulting image blocks, the average forward overlaps were 70%, the side overlaps were 75%, and the ground sample distance (GSD) was approximately 0.50 m. The weather conditions were partly cloudy during the campaign.

The FPI camera was operated in the wavelength range of 500–900 nm (from visible green to near-infrared). The number of spectral bands was originally 41, but after the laboratory calibration correction (Mäkynen et al., 2011) only 24 bands remained (see details in Section 2.3). The full width at half maximum (FWHM) of the bands varied between 12 and 30 nm (Fig. 2). The exposure time was 6 ms.

Two portable reflectance reference targets, 5 m × 5 m in size and with a nominal reflectance of 0.10 and 0.25, were installed in the flight area for the reflectance transformations. Furthermore, a grass field near the targets was used as the reflectance reference.

The UAV flights were carried out in the Kerinkallio area and in the Mukkula area using the FPI camera on August 23, 2013 (Näsi et al., 2015); the spectral settings were similar to the settings used for the aircraft data. The coverage of UAV flights were 4.2 ha and 3.6 ha in Kerinkallio and Mukkula, respectively. Thus, the areas were significantly smaller than the aircraft areas (Table 2, Fig. 1). The UAV images with a nominal GSD of 0.10 m were highly detailed and even branch-level details were visible (Fig. 3) due to a low flying height of 90 m (Table 2). Individual trees could also be identified in the aircraft images having a GSD of 0.50 m, but the branch-level details were not visible.

Hundreds of small-format images (Table 2) were collected to cover the areas of interest. A rigorous pre-processing workflow has been developed for the datasets in previous studies (Honkavaara et al., 2013). The following sections describe the details of the processing phases, including orthophoto mosaic generation and further steps taken for feature extraction, classifier training, and producing a spruce health map.

2.3. Mosaic generation

The mosaic generation phases included geometric processing, radiometric correction, and mosaic calculation.

Geometric processing included determining the image orientations and band-matching to align individual bands of the hyperspectral data cubes. The latter process was necessary because of the time-sequential imaging principle of the FPI camera. We chose one band for calculating the orientations of the FPI data cubes (band 14: L0 = 626.3 nm). Exterior orientations were determined by self-calibrating the bundle block adjustment using Socet GXP (BAE Systems, San Diego, USA) commercial software. The georeferencing was based on national open topographic datasets (NLS, 2016), the orthophoto, and a national ALS-based digital surface model (DSM). A total of 19 photogrammetric control points for the south area and 17 control points for the north area were identified from the datasets using manual measurements. The adjustment results indicated good geometric accuracy of approximately 1 m for the dataset. For the band alignment, band 14 was used as the reference band. All bands were matched to the reference band using a feature-based matching algorithm, and an affine transformation was used to map the bands to the reference band (Honkavaara et al., 2013).

The radiometric correction process started with the radiometric sensor corrections determined in a laboratory calibration, which included the photon response nonuniformity correction (PRNU) and the spectral smile correction (Mäkynen et al., 2011). Other correction steps were carried out using in-house radiometric processing software (Honkavaara et al., 2013). We used the empirical line method (Smith and Milton, 1999) to calculate the transformation from DNs to reflectance with the aid of the calibrated reflectance reference targets. Due to the variable weather conditions and other radiometric phenomena, additional radiometric corrections were necessary in order to make the image mosaics uniform. Both datasets included a few dark images because of cloud shadows; those images were removed during the processing phase (25 images in the north area and 12 images in the south area). To compensate for further radiometric disturbances, a radiometric block adjustment method was used to determine the model-based radiometric correction. In this investigation, the relative radiometric differences between the images and the disturbances caused by the object reflectance anisotropy (bidirectional reflectance distribution function, BRDF) were modeled and resolved during the radiometric modelling process in order to transform the datasets radiometrically to the reflectance scale corresponding to the nadir view geometry (see details in Honkavaara et al., 2013).

Orthorectified reflectance mosaics were calculated using the aircraft images with a GSD of 0.50 m by utilizing the DSMs, orientation information, and radiometric model. The DSMs were created using dense digital image matching techniques from the RGB image data (GSD: 0.05 m), which was collected on the same day as the hyperspectral data. The resulting mosaics showed good radiometric uniformity, and the geometric accuracy was on the level of 1 m (Fig. 1).

The processing chain for the UAV image data was similar to the one for the aircraft data, including making the sensor corrections, determining the image exterior orientations, generating the DSM,

Table 2
Details of the FPI image blocks (GSD: ground sample distance; overlap f;s: forward and side overlaps of photogrammetric image block; N HC: number of hypercubes).

Area	Platform	GSD (cm)	Flying altitude	Time (UTC + 3)	Solar elevation	Sun azimuth	Expo-sure (ms)	Overlap f;s (%)	N HC
North	aircraft	50	500	13:48–13:55	32.3	191.4	6	70, 75	40
South	aircraft	50	500	13:57–14:14	31.80	195.8	6	70, 75	228
Mukkula	UAV	9	90	10:29–10:35	31.88	130.06	6	55, 55	96
Kerinkallio	UAV	9	90	13:48–13:55	40.01	190.27	8	55, 55	80

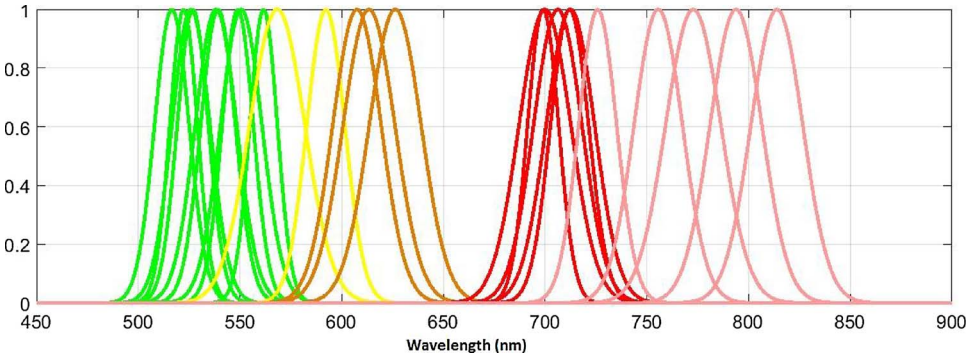

Fig. 2. Spectral settings of the FPI camera showing the central wavelengths and the FWHM for each band. Colors show in which part of the spectrum the band is located. Pink is used for the bands in the near infra-red region that are not visible to the human eye.

calculating the radiometric model parameters, and calculating the orthophoto mosaic. In this case, the image orientations and DSMs were determined using Agisoft PhotoScan professional commercial software (AgiSoft LLC, St. Petersburg, Russia); the radiometric corrections were carried out using the same approach as with the aircraft images. The outputs were reflectance mosaics with a GSD of 0.10 m in Kerinkallio and a GSD of 0.12 m in Mukkula. More details are given by Näsi et al. (2015).

The result of the mosaic generation process were the hyperspectral mosaics named North and South for the aircraft areas and Kerinkallio and Mukkula in the UAV datasets. The UAV and aircraft datasets were radiometrically and geometrically comparable because both datasets were captured with the same sensor and with a nadir viewing geometry using an airborne platform. Furthermore, rigorous methods and calibrated reflectance panels were used to calculate the georeferenced reflectance output products. However, due to different GSDs the pixel of aircraft data included approximately 5 × 5 UAV pixels (Fig. 3), which causes spectral mixing.

2.4. Spectrum and feature extraction

Spectral features were calculated based on the image mosaics (Section 2.3) for each individual tree based on their coordinates. We used the same features as Näsi et al. (2015):

1. The original 24-band spectra;
2. Three different normalized channel ratios (vegetation indices; VI) were computed using the reflectance (R) of two bands:

$$VI_1 = (R_{793.8} - R_{626.3})/(R_{793.8} + R_{626.3}),$$
$$VI_2 = (R_{772.8} - R_{725.8})/(R_{772.8} + R_{725.8}),$$
$$VI_3 = (R_{550.6} - R_{626.3})/(R_{550.6} + R_{626.3}). \quad (1)$$

The bands were selected based on class separability analysis, which was evaluated based on the differences between the full spectra of various crown color classes; this was based in turn on the analysis of variance (ANOVA) (Näsi et al., 2015).

Our approach was to use a single spectral feature for each individual tree (instead of using spectral features of each pixel in the tree crown area). In the case of the aircraft data, the GSD was 0.50 m, and each tree consisted of 3–25 pixels depending on the size of the tree crown. We used a 3 × 3 pixel window for calculating the spectral features. We likewise used the average of the pixels and the average of the three brightest pixels in the window to derive the spectral features. In the case of the UAV data, there were more pixels related to each tree than in the aircraft data due to small GSD of 0.10–0.12 m (Fig. 2). Thus the spectral feature extraction was done using a circular window with a 1 m radius; either the average over the entire area or six brightest pixels were used. The approach using the brightest pixels was of interest, since the arithmetic mean might not be the ideal feature due to the shadow pixels in the window. A similar approach was also used by Campbell et al. (2004).

For the methods based on individual tree analysis, it is crucial that the coordinates of the reference trees correspond to the correct trees in the images. Our visual assessment indicated that there was a minor positional discrepancy between the orthophoto mosaics and the coordinates of the reference trees measured in field. We aligned the datasets interactively; small systematic shifts of 1–10 m for the entire

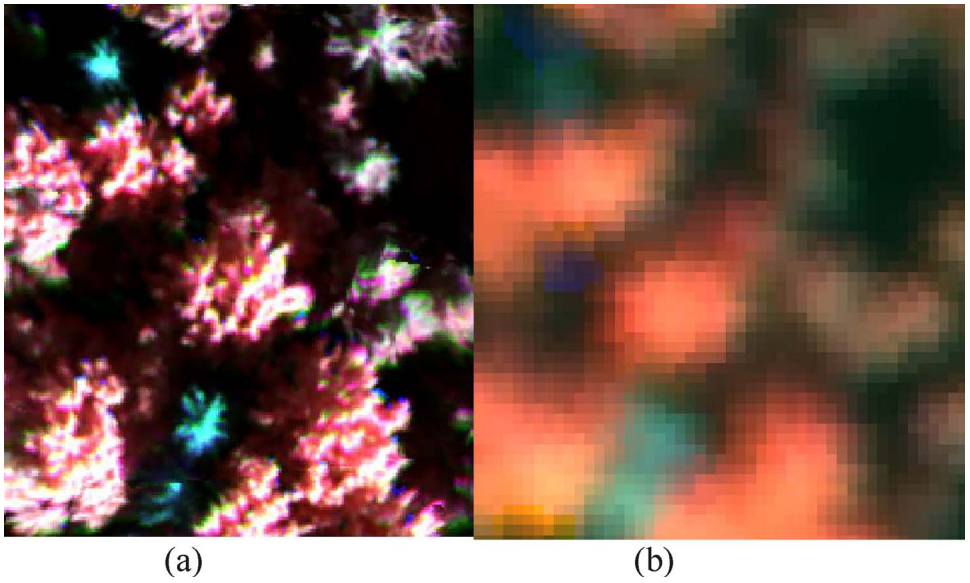

Fig. 3. Examples of images captured by the UAV (a) with a GSD of 10 cm and the aircraft (b) with a GSD of 50 cm.

group of treetops in each sample plot were necessary. The potential reasons for the mismatches could be inaccuracy in the GPS measurements for the centers of the sample plots during the field survey, different positioning of the tree trunk on the ground level and from the air, or geometric errors in the image mosaics. All reference plots were checked interactively to ensure that after the alignment process, the reference trees corresponded correctly to the trees in the remote sensing datasets.

It was necessary to investigate whether the tree size had an impact on the spectra. We divided the trees into four groups based on their dbh (< 30 cm, 30–40 cm, 40–50 cm, > 50 cm) and calculated the average and standard deviation of the spectra in each group. The numbers of samples in each group were 60, 167, 87, and 16, respectively. These four groups resulted in a total of six 2-pair combinations. The spectral similarity was tested using a *t*-test, with two samples assuming equal variances. The P-values were over 0.05 for every comparison, except for five bands in the comparison of groups with 30–40 cm and 40–50 cm of dbh. This result indicated that the tree size did not significantly affect the spectra used in this study; thus, it was not necessary to account for the tree size in the analysis.

2.5. Training and assessing the classifier employing the reference plots

A support vector machine (SVM) classifier was used for the classification phase. SVM has yielded good classification results for hyperspectral data compared to other classifiers (Cracknell and Anya, 2014). We used the LIBSVM tool and its C-SVM version, as proposed by Chang and Chih-Jen (2011). First, it was necessary to scale the features to the same scale, between 0 and 1, to avoid numerical problems. We applied the Radial Basis Function (RBF) as the kernel, as suggested by Hsu et al. (2010). For optimizing the RBF parameters C (complexity) and γ (kernel width), we used a 2D grid-based, cross-validation search.

The reference data was imbalanced: the majority of the training samples were from the healthy and dead classes, whereas only a few samples were from the infested class (Table 1). Imbalance can reduce the overall accuracy unless accounted for in the classifier (Sun et al., 2009). The SVM classifier attempts to maximize the overall accuracy and gives the same cost for every sample in the basic mode, similar to many other classifiers (Cao et al., 2013). Possible approaches to compensate for the problem of imbalance include using different minimization cost functions for each class or weighting the cost value for the classes in a different way. For SVM, special class-imbalanced classifiers or resampling methods have been proposed (Cao et al., 2013). We used the method suggested by Ben-Hur and Weston (2010) to assign different costs for misclassification (weighting) to each class such that the total cost for each class is equal.

The spectral reflectance features were in the range of [0,1], and the VI-features (equation 1) were in the range of [−1,1]. We also tested scaling the VI-features individually to the range of [0,1] to study their impacts on the classification results.We used three different reference data combinations to train and validate the classifier:

- Combination 1. The features of all the reference trees in the aircraft area (set 1 + set 2, 330 trees) were used to train and validate the classifier.
- Combination 2. The features from the Mukkula and Kerinkallio UAV and aircraft datasets (set 1, 78 trees) were used to train and test the classifier, and the aircraft data (set 2, 252 trees) was used for validating it.
- Combination 3. The third combination was similar to the second combination, except the aircraft features of set 1 were used for validating purposes.

The leave-one-out cross validation method was applied for each combination to assess the classifier's performance; the hold-out method was applied for combinations 2 and 3 to assess the performance of the SVM classifier in the full area. Based on the validation data, we calculated the confusion matrix and Cohen's kappa value as well as the producer's accuracies and overall accuracies of the classifier.

2.6. Production of spruce health maps

An individual tree-based approach was used to calculate spruce health maps for the entire area using the aircraft data. The steps in this procedure included detecting individual trees, classifying tree health, and generating a map.

We used the remote sensing dataset to detect trees because an individual tree-based GIS was not available for the area. This approach had its limitations because the campaign was not designed for individual tree detection and tree species classification. In this study, we assumed that all detected trees were Norway spruces. This was a quite feasible assumption because the vast majority of the trees in the study area were Norway spruce (85% of the analyzed trees); furthermore, users of the maps are asked to be careful when interpreting the results. In the future, the existing individual tree-based GIS will replace this step.

Image brightness information from the reflectance mosaics was used to detect the trees. The approach is based on the assumption that image brightness in the upper parts of the tree tops is greater than in the lower parts, which obtain less illumination or are in shadow, and individual bright treetops can thus be identified. The GSD of 0.5 m provided approximately 10 pixels in mature trees, which was sufficient for identifying trees (Fig. 4a). The algorithm included the following steps:

1. Classify the reflectance mosaics into 25 classes based on the pixel brightness information using the unsupervised k-means classifier (Kotsiantis et al., 2007) (Fig. 4b). In the classified image, the brightest treetops belong to class 25 and the darkest shadows to class 1, while other brightness levels are assigned to classes in between these two.

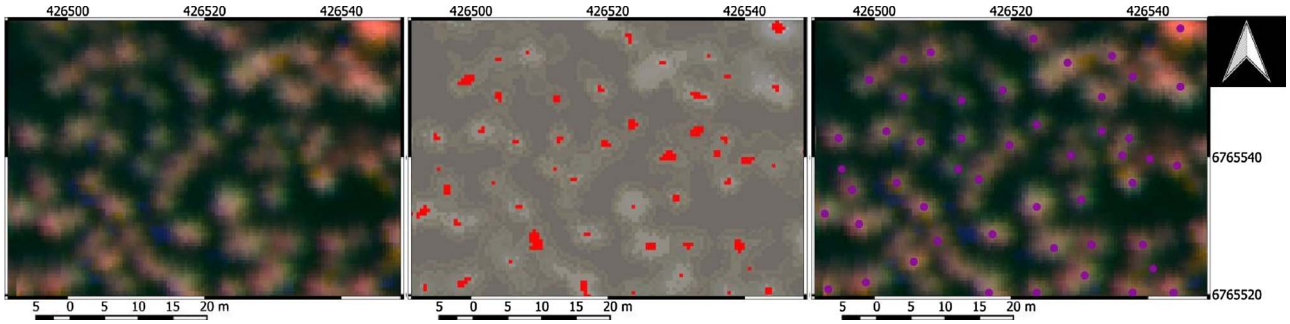

Fig. 4. (a) Part of the reflectance mosaic with color-infrared bands. (b) Results of classification into 25 classes using the unsupervised k-means classifier. Red pixels show the areas where the local maxima were identified. (c) Central coordinates of the maxima were labelled as treetops. (For interpretation of the references to colour in this figure legend, the reader is referred to the web version of this article.)

2. Filter the image based on the 25 classes (created in step 1) using a 2-D Gaussian smoothing kernel (Babaud et al., 1986) with a standard deviation of 1.0.
3. Find each local maximum in 8-connected neighborhoods based on the classified image using the Matlab™ function imregionalmax (Fig. 4b, red).
4. Take the central coordinates of the local maxima as treetops (Fig. 4c).

In the classification step, the spectral and index features were extracted for the detected trees in the same way as for the reference trees (Section 2.4). Then, the identified trees were classified with the SVM classifier using combination 1 (all 330 reference trees, aircraft) for training. Finally, the spruce health maps were produced for the north and south areas using three (healthy, infested, dead) and two (healthy, dead) different health classes.

3. Results and discussion

3.1. Spectral data of the reference trees

The average spectra for each tree color class for the aircraft data were calculated in the image window of 3 × 3 pixels and using the average of the three brightest pixels (Fig. 5). The strategy of using an average of the three brightest pixels (Fig. 5a) provided better separation of the crown color classes in comparison to the averaged spectra for the entire dataset (Fig. 5b), as also noted by Näsi et al. (2015) with reference to UAV data (Fig. 5c,d). We thus used the features with an average of the three brightest pixels for the next analysis steps. In comparison to the results from UAV images with 0.10 and 0.12 m GSDs (Näsi et al., 2015), the separation of healthy and infested classes were similar to the results from the UAV data when using the average for an image window with a 1 m diameter. This is a consistent result because the area of three pixels in the aircraft data (0.75 m^2; Fig. 5a) corresponds to the UAV window size (0.79 m^2; Fig. 5d).

3.2. Classification results for the reference plots

The classification results for the reference plots are presented in following sections (Tables 3–5) for individually scaled data (scaling), for weighted cost based on the number of samples (weighting), and when using both scaling and weighting (both). The results are discussed below with respect to the separability of different tree health classes, the impact of the spatial resolution, and the impact on the number of reference trees.

3.2.1. Separability of different classes

When using only the two classes healthy and dead (combination 1), we obtained a good classification result with an overall accuracy of 93% (kappa: 0.77) with weighted misclassification costs and spectrum features (Table 3). The classification accuracy was almost as good using scaled indices as features (overall accuracy of 92%, kappa: 0.75).

With three infestation classes, the classification accuracy was poorer than the result obtained from the two-class classification. Our assessment of the spectra indicated that the separation of the infested and healthy trees was quite poor (Fig. 5), thus affecting the accuracy. The best overall accuracy, 87% (kappa: 0.61), was gained with scaled indices features. However, the class of infested trees remained unidentified. For this reason, we consider the classification system with weighted spectrum features, which provided an accuracy of 35% for the

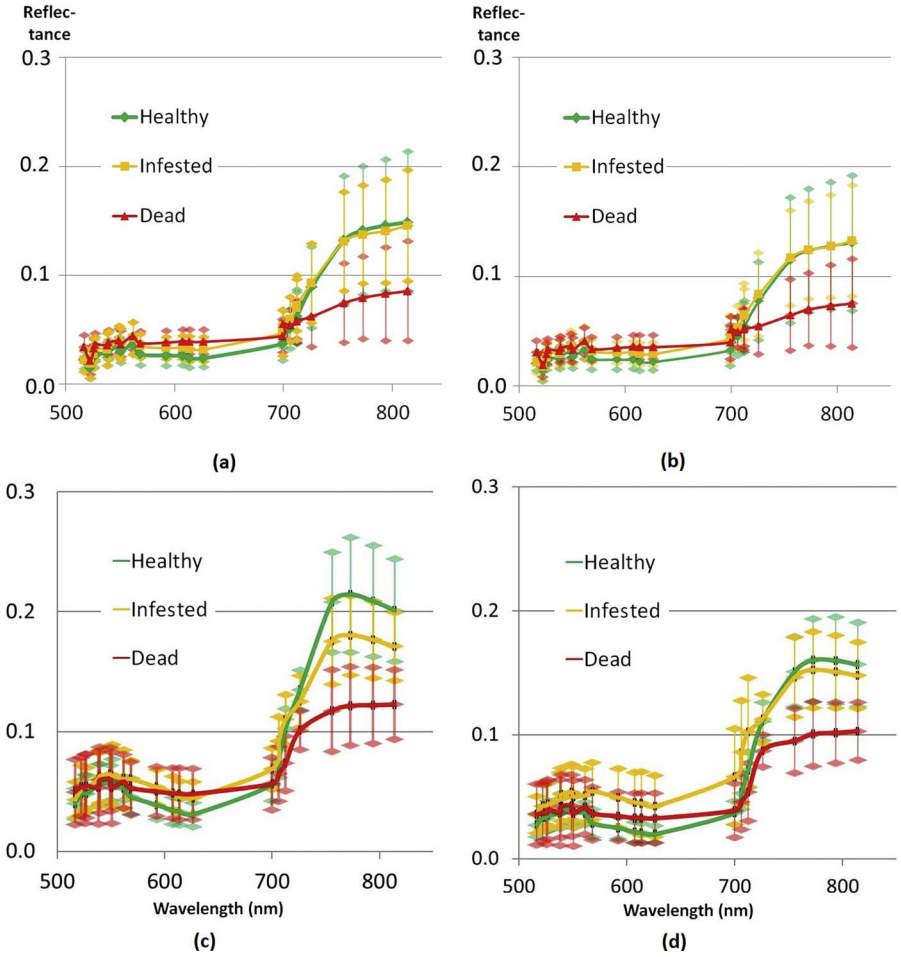

Fig. 5. Average spectra with standard deviation bars of the healthy, infested, and dead reference trees. Aircraft spectra based on an image window of size of 3 × 3 pixels: (a) average of the three brightest pixels and (b) average of all the pixels. UAV spectra from Kerinkallio: (c) average of the six brightest pixels (d) and average of all the pixels (original source of images c and d: Näsi et al., 2015).

Table 3
SVM Classification results for combination 1, where aircraft features of the reference trees (set 1 + set 2) were used as training data (the results are shown for 2 classes (healthy and dead) and for 3 classes (healthy infested and dead); weighting: use of cost functions based on the number of samples in the three classes; scaling: every feature scaled individually to a range of 0–1; leave-one-out technique was used for validation, with the best results presented in bold).

Features	Weighting/ Scaling	N of classes	Producer's accuracies (%) Healthy	Infested	Dead	Overall accuracy (%)	Kappa
Spectrum	Both	2	92		73	88	0.65
Indices			89		80	87	0.64
Spectrum	Scaling		94		72	89	0.67
Indices			98		72	92	0.75
Spectrum	Weighting		**96**		**80**	**93**	**0.77**
Indices			87		75	85	0.57
Spectrum	Both	3	92	10	67	82	0.52
Indices			80	45	70	76	0.50
Spectrum	Scaling		92	15	67	83	0.55
Indices			98	0	72	87	0.61
Spectrum	Weighting		**83**	**35**	**78**	**79**	**0.54**
Indices			74	30	70	71	0.40

Table 4
Results of reference data set 1 (the leave-one-out method was used for validation, with the best results presented in bold).

Dataset Description	Features	Weighting/ Scaling	Producer's accuracies (%) Healthy	Infested	Dead	Overall accuracy (%)	Kappa
Training: UAV, Leave-one-out, Combination 2	Spectrum	Both	75	40	89	73	0.57
	Indices		**86**	**67**	**81**	**81**	**0.70**
	Spectrum	Scaling	72	40	89	72	0.55
	Indices		86	47	81	77	0.63
	Spectrum	Weighting	75	60	89	77	0.64
	Indices		83	60	81	78	0.66
Training: aircraft, Leave-one-out, Combination 3	Spectrum	Both	78	40	78	71	0.53
	Indices		54	73	65	57	0.27
	Spectrum	Scaling	**86**	**40**	**74**	**73**	**0.56**
	Indices		94	00	81	72	0.51
	Spectrum	Weighting	83	00	44	54	0.19
	Indices		67	00	85	60	0.36

Table 5
Results of reference data set 1 and set 2 (training was performed using features from set 1 and assessed using features from set 2 with the hold-out validation method, with the best results presented in bold).

Dataset Description	Features	Weighting/ Scaling	Producer's accuracies (%) Healthy	Infested	Dead	Overall accuracy (%)	Kappa
Training: UAV, Testing: aircraft, Hold-out, Combination 2	Spectrum	Both	50	0	83	52	0.16
	Indices		**89**	**47**	**58**	**81**	**0.51**
	Spectrum	Scaling	54	0	85	56	0.21
	Indices		95	20	45	82	0.53
	Spectrum	Weighting	23	73	83	36	0.15
	Indices		64	60	75	36	0.37
Training: aircraft, Testing: aircraft, Hold-out, Combination 3	Spectrum	Both	67	7	85	66	0.31
	Indices		58	20	85	60	0.38
	Spectrum	Scaling	64	0	98	63	0.32
	Indices		99	0	00	77	0.01
	Spectrum	Weighting	98	0	43	83	0.38
	Indices		**87**	**33**	**68**	**80**	**0.51**

infested trees and an overall accuracy of 79% (kappa: 0.54), the most successful of the three class-based analyses (Table 3).

3.2.2. *Effect of spatial resolution*

A comparison of the results from combinations 2 and 3 made it possible for us to consider the effects of spatial resolution on the classification results. We used reference tree set 1 for these combinations; the difference was that the UAV data with a 0.10 m GSD was used in combination 2, while the aircraft data with a 0.50 m GSD was used in combination 3. The best classification result from combination 2 provided an overall accuracy of 81% (kappa: 0.70). The best result from combination 3 was 73% (kappa: 0.56, Table 4). Producer's accuracies for the infested and dead trees were better with combination 2 (67% and 81%) than with combination 3 (40% and 74%). For the healthy trees, the accuracy was the same (86%) in both combinations. The classification accuracy for the infested trees was better in almost every case with the UAV data (combination 2). This result indicates that the use of higher spatial resolution data may provide higher classification accuracy. Previous studies have yielded similar results. For example, Lausch et al. (2013) investigated the effects of spatial resolution on the accuracy in bark beetle damage classification with much larger GSDs (4 m and 7 m). The smaller GSD (4 m) provided better classification accuracy. This is a logical result; better results with higher resolutions are likely to be due to the lower level of mixing of spectra from adjacent objects.

3.2.3. Effect of number of reference trees and training data

In combination 1, we used all of the reference plots (set 1 + set 2) for training the classifier. The best overall accuracy was 79% (kappa: 0.54) (Table 3). When comparing these results to combination 3, where set 1 was used for training and set 2 for validation (features from aircraft data), we found that the accuracy of the classification was at the same level (overall accuracy 80%, kappa: 0.51), indicating that the smaller training sample was sufficient (Table 5). The hold-out-estimation results from combination 2 (training using features derived from the UAV data and validation using the aircraft features) provided an overall accuracy of 81% (kappa: 0.51; Table 5), which was at the same level as with combination 3, even though the classifier training was based on spectral data captured from a different platform at a different time. We obtained the best accuracies in combination 2 using scaling and indices, which was the expected result because they eliminated the effects of different spectrum levels and only the shape of the spectrum had an impact.

This result suggests that with an individual tree-based approach, the training of the classifier for a large area could be performed using training data from a smaller, representative area. This is a logical and favorable result for individual tree-based remote sensing. When spectra are collected from the tree crown area, only the spectral information on spruce trees needs to be considered. Thus, we did not need to account for the background effects caused by different soils and understory, which is typically required when using area or pixel-based approaches (Fassnacht et al., 2014). Furthermore, the phenological variations must be accounted for. For example, if we are capturing data annually at the end of the growing season, the phenological variations will have only a minor contribution. A further requirement for reliable results is good calibration of the remote sensing data. The utilization of spectral libraries could also be feasible with the individual tree-based approach.

3.3. Production of spruce health maps

The objective of this section is to demonstrate tree health mapping of the entire studied area. The classification accuracies reported in Section 3.2 are not valid for these maps, which were composed by classifying the trees detected during the image analysis. The detected trees therefore include species other than spruces (15% of species were other than spruces), whereas not all of the spruces may have been detected by our algorithm. The following results can thus only be considered as a demonstration of how to generate health maps over larger areas.

We detected a total of 30,944 trees within the entire research area when using the procedure described in Section 2.6. Our visual assessment of the health maps indicated that the large and separable trees, such as most of the Norway spruces (Fig. 4) could be detected quite successfully with the method. However, identification of small trees in the suppressed canopy cover layer was poor. We also noticed that identification of deciduous trees forming a continuous canopy surface was not accurate either. We conducted a numerical evaluation of the identification rate by comparing the coordinates of the reference trees with the detected trees. We found 65% of the reference trees when using a 3 m search radius.

We classified all of the detected trees using combination 1 indices without scaling features and with the weighting based on the number of samples. These feature selections provided relatively good classification accuracy for all classes (Table 3). For the three-class case, 65.1% of the trees were classified as healthy, 26.5% as infested, and 8.4% as dead (Fig. 6a,c). When only two classes were used, 82.4% of trees were classified as healthy and 17.6% as dead. It could be expected that broadleaved trees were classified into the class of healthy spruce trees. Their spectra were closer to that of healthy spruces than to other classes. There were also a few Scots pines (*Pinus sylvestris* L.) in the research area. These trees were mostly classified as healthy as well. Visual evaluation of the results confirmed these considerations.

Visual assessment of the spruce health maps revealed hotspot areas of infestation, that is to say, areas with a large number of infested and dead trees. In the best cases, the identified infested or dead trees matched well with the ground-truth data. However, in the western part of the south area (Fig. 6c,d), a major portion of the trees classified as infested in the three-class case were classified as dead in the two-class case. An overestimation of dead spruces is, however, more preferable than an underestimation of dead spruces. The maps may give a quick overall view of the infestation situation for forest management purposes.

4. Summary and outlook

We investigated the potential of novel remote sensing technologies to evaluate tree health at the individual tree level in urban areas. We classified spruces and received the best overall accuracy of 93% (kappa: 0.77) for two color classes (healthy, dead) in the entire study area covered by the aircraft dataset. When using the classes healthy, infested, and dead in a smaller sub-area, the finer spatial resolution UAV dataset provided better results, with an overall accuracy of 81% (kappa: 0.70), than did the aircraft dataset, which provided an overall accuracy of 73% (kappa 0.56). Identifying the infested class was the most troublesome aspect of the investigation. Furthermore, we showed that the method was quite insensitive to the number and distribution of training data; in this sense, the individual tree-based approach had the advantage of minimizing background influences when focusing the spectral analysis on the tree crowns. These results are very promising; thus, the method developed in this study can be seen as an efficient tool for timely updating and monitoring the health status of an urban forest at the individual tree level.

Most recent studies have used lower spatial resolution data or an area-based approach (Lausch et al., 2013; Fassnacht et al., 2014; Lehmann et al., 2015; Foster et al., 2016). The advantage of the individual tree-based approach is that, ultimately, it provides a new level of precision and efficiency for forest health management practices. In sensitive urban forests, precision forestry is a highly attractive approach. The basis for such an approach is GIS with individual tree information, such as the tree positions and species, which have been produced based on a multisource inventory (Holopainen et al., 2014). Then, low-cost remote sensing tools can be used to assess and monitor tree health. If individual tree-level information is not available, the remote sensing campaign should be designed to support individual tree detection, tree species classification, and tree health assessment at a sufficient level of quality.

There are still many options for further developing the method used in this study. With the low-cost technologies now available, multitemporal monitoring can be done in a cost-effective manner. In the case of continuous multi-temporal forest health monitoring, methods detecting changes can reveal new infestations (Senf et al., 2017). Other spectral ranges, particularly short-wave-infrared (SWIR) (Foster et al., 2016; Abdullah et al., 2018) or thermal (Junttila et al., 2016), can provide additional information on the health status of a forest.

It is worth noting that our remote sensing datasets were demanding. The UAV and aircraft datasets were collected on different dates, which could have caused some differences in the spectral values. However, the spectra of mature spruces could be expected to be relatively stable because the data capture was carried out in the end of the growing season. We used an advanced and rigorous radiometric processing approach (Honkavaara et al., 2013), but even still disturbances might have reduced the accuracy of the results. Furthermore, uncertainties related to the fieldwork might also have impacted the results and quality assessment. The classification of Norway spruces in the field was conducted over a span of four weeks in August. Weather and light conditions varied from clear and sunny to gentle rain during the field data capture. The visual crown color assessment can be affected by such conditions, even though the observers were highly experienced.

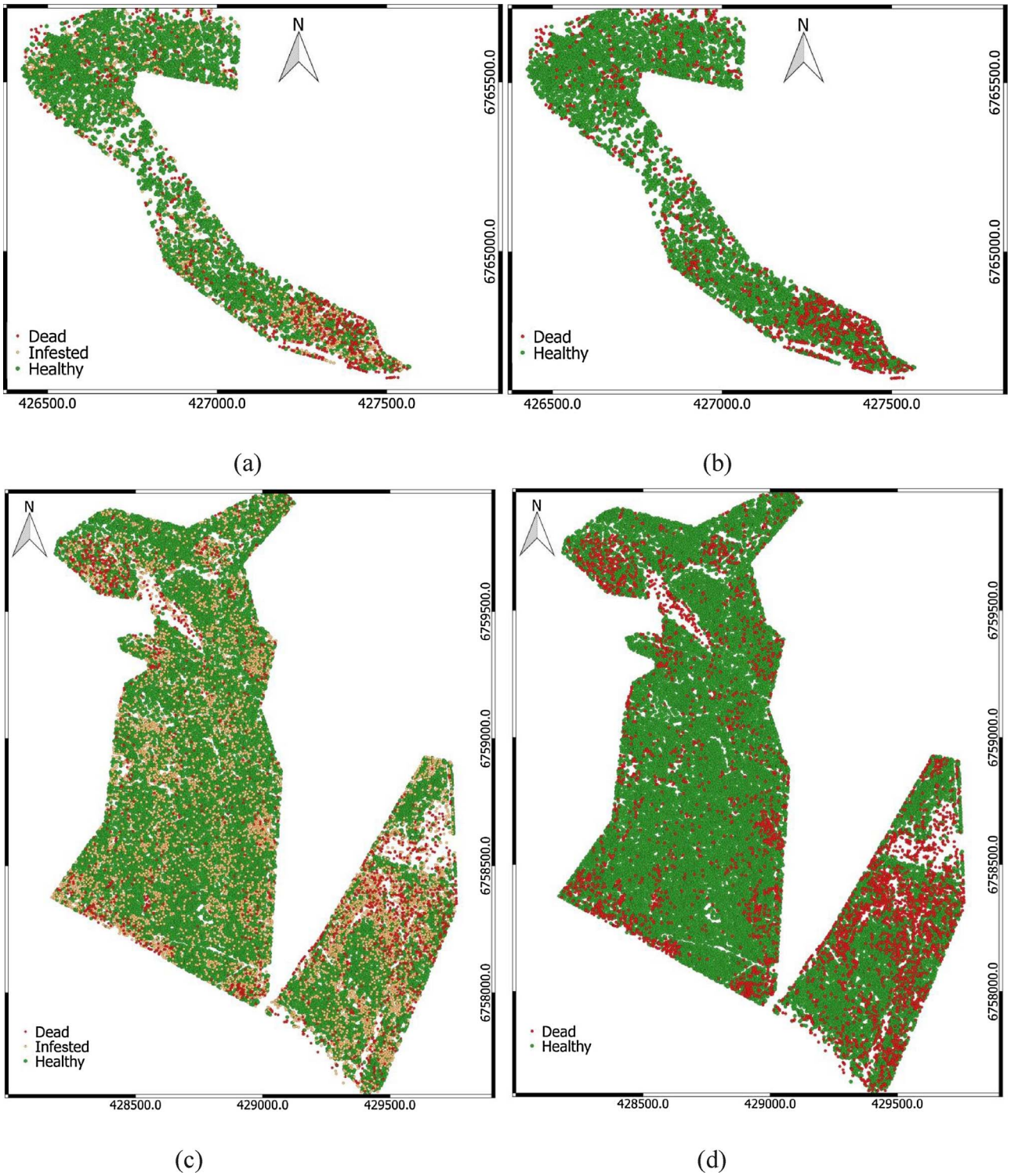

Fig. 6. Individual spruce health maps are shown for the north area (a, b) and the south area (c, d) using three classes (a, c) and two classes (b, d) for classification.

Additionally, the time gap between the first field assessments and the aircraft data may already show a gradual deterioration of a tree crown between those two dates. Despite the uncertainties, these results can be considered very promising.

We expect that in the near future, the major part of the laborious and costly fieldwork process could be replaced with cost-efficient, remote sensing-based tools. The low-cost UAV tools could even be operable by the managers of urban forests themselves. These results indicate that in the future, such remote sensing tools will allow for rapid and well-honed methods for planning and decision-making in cases of forest disturbances and ultimately digitalization of the forest health management practices. Precise and rapid management operations are important particularly in the early phases of *I. typographus* colonization to prevent a widespread outbreak.

5. Conclusion

This investigation developed an affordable remote sensing-based

method for monitoring tree health to support the forest management needs of small-scale areas, such as urban forests. Our method utilized photogrammetry and hyperspectral imaging to identify the status of bark beetle infestation of Norway spruce at the individual tree level. A novel, low-cost hyperspectral camera was used as the predominant sensing method from UAV and aircraft platforms. Data from both systems was suitable for detecting the health status of spruce trees, but the UAV-based results were more accurate, which is likely because of the finer spatial resolution and lower level of spectral mixing. The results of the aircraft based data showed that using a small subset of features for training provided almost as good results as using the full dataset. Furthermore, training the classifier using the higher spatial resolution, UAV-based spectral features provided similar classification results as the use of lower spatial resolution, aircraft-based features. These results suggest that when combining calibrated spectral information about different infestation levels based on close-range UAV or laboratory measurements with well-calibrated remote sensing hyperspectral imagery and individual tree-based analysis, cost-efficient remote sensing tools requiring a minimal amount of field work can be developed. Reducing the need for expensive and time-consuming fieldwork and using low-cost remote sensing tools enables affordable and rapid environmental monitoring and corresponds to the increasing forest health management needs of urban areas.

Acknowledgments

This work was funded by the MMEA research program, coordinated by Cleen Ltd. (Helsinki, Finland), with additional funding from the Finnish Funding Agency for Technology and Innovation, Tekes, and the Academy of Finland (grant number 273806). The project was also funded by the Niemi Foundation and the Maj and Tor Nessling Foundation. We are grateful to Lentokuva Vallas Oy for the aircraft data capture. We wish to thank M.S. Anna-Maaria Särkkä, head of the forestry unit in the city of Lahti, for her cooperation. We like to thank Lauri Markelin and Kimmo Nurminen for assistance in the remote sensing campaigns and Sini Keinänen during the fieldwork.

References

Aasen, H., Burkart, A., Bolten, A., Bareth, G., 2015. Generating 3D hyperspectral information with lightweight UAV snapshot cameras for vegetation monitoring: from camera calibration to quality assurance. ISPRS J. Photogramm. Remote Sens. 108, 245–259.

Abdullah, H., Darvishzadeh, R., Skidmore, A.K., Groen, T.A., Heurich, M., 2018. European spruce bark beetle (Ips typographus, L.) green attack affects foliar reflectance and biochemical properties. Int. J. Appl. Earth Obs. Geoinf. 64, 199–209.

Alvey, A.A., 2006. Promoting and preserving biodiversity in the urban forest. Urban For. Urban Green. 5 (4), 195–201.

Aukema, J.E., Leung, B., Kovacs, K., Chivers, C., Britton, K.O., Englin, J., Frankel, S.J., Haight, R.G., Holmes, T.P., Liebhold, A.M., McCullough, D.G., Von Holle, B., 2011. Economic impacts of non-native forest insects in the continental United States. PLoS One 6 (9), e24587. http://dx.doi.org/10.1371/journal.pone.0024587.

Babaud, J., Witkin, A.P., Baudin, M., Duda, R.O., 1986. Uniqueness of the Gaussian kernel for scale-space filtering. IEEE Trans. Pattern Anal. Mach. Intell. 1, 26–33.

Ben-Hur, A., Weston, J., 2010. A User's Guide to Support Vector Machines. Data Mining Techniques for the Life Sciences. pp. 223–239.

Cajander, A.K., 1926. The theory of forest types. Acta For. Fenn. 29, 1–108.

Campbell, P.E., Rock, B.N., Martin, M.E., Neefus, C.D., Irons, J.R., Middleton, E.M., Albrechtova, J., 2004. Detection of initial damage in Norway spruce canopies using hyperspectral airborne data. Int. J. Remote Sens. 25, 5557–5584.

Cao, P., Dazhe, Z., Osmar, Z., 2013. An optimized cost-sensitive SVM for imbalanced data learning. Advances in Knowledge Discovery and Data Mining. Springer Berlin Heidelberg, pp. 280–292.

Chang, C.-C., Chih-Jen, L., 2011. LIBSVM: a library for support vector machines. ACM Transactions on Intelligent Systems and Technology (TIST) 2.3. pp. 27. Software available at http://www.csie.ntu.edu.tw/~cjlin/libsvm.

Cracknell, M.J., Anya, M., 2014. Reading geological mapping using remote sensing data: a comparison of five machine learning algorithms, their response to variations in the spatial distribution of training data and the use of explicit spatial information. Comput. Geosci. 63, 22–33.

Dash, J.P., Watt, M.S., Pearse, G.D., Heaphy, M., Dungey, H.S., 2017. Assessing very high resolution UAV imagery for monitoring forest health during a simulated disease outbreak. ISPRS J. Photogramm. Remote Sens. 131, 1–14.

Fassnacht, F.E., Latifi, H., Ghosh, A., Joshi, P.K., Koch, B., 2014. Assessing the potential of hyperspectral imagery to map bark beetle-induced tree mortality. Remote Sens. Environ. 140, 533–548.

Foster, A.C., Walter, J.A., Shugart, H.H., Sibold, J., Negron, J., 2016. Spectral evidence of early-stage spruce beetle infestation in Engelmann spruce. For. Ecol. Manage. 384, 347–357.

Göthlin, E., Schroeder, M., Lindelöw, Å., 2000. Attacks by Ips typographus and Pityogenes chalcographus on windthrown spruces (*Picea abies*) during the two years following a storm felling. Scand. J. For. Res. 15 (5), 542–549.

Ghimire, R.P., Kivimäenpää, M., Blomqvist, M., Holopainen, T., Lyytikäinen-Saarenmaa, P., Holopainen, J.K., 2016. Effect of bark beetle (*Ips typographus* L.) attack on bark VOC emissions of Norway spruce (*Picea abies* Karst) trees. Atmos. Environ. 126, 145–152.

Hall, R.J., Castilla, G., White, J.C., Cooke, B.J., Skakun, R.S., 2016. Remote sensing of forest pest damage: a review and lessons learned from a Canadian perspective. Can. Entomol. 1–61.

Havasová, M., Bucha, T., Ferencík, J., Jakus, R., 2015. Applicability of a vegetation indices-based method to map bark beetle outbreaks in the High Tatra Mountains. Ann. For. Res. 58 (2), 295.

Holopainen, M., Vastaranta, M., Hyyppä, J., 2014. Outlook for the next generation's precision forestry in Finland. Forests 5 (7), 1682–1694.

Honkavaara, E., Saari, H., Kaivosoja, J., Pölönen, I., Hakala, T., Litkey, P., Mäkynen, J., Pesonen, L., 2013. Processing and assessment of spectrometric, stereoscopic imagery collected using a lightweight UAV spectral camera for precision agriculture. Remote Sens. 5, 5006–5039.

Hsu, C.W., Chang, C.C., Lin, C.J., 2010. A Practical Guide to Support Vector Classification. Available: https://www.cs.sfu.ca/people/Faculty/teaching/726/spring11/svmguide.pdf.

Junttila, S., Vastaranta, M., Hämäläinen, J., Latva-käyrä, P., Holopainen, M., Hernández Clemente, R., Hyyppä, H., Navarro-Cerrillo, R.M., 2016. Effect of forest structure and health on the relative surface temperature captured by airborne thermal imagery—case study in Norway spruce-dominated stands in Southern Finland. Scand. J. For. Res. 1–12.

Kärvemo, S., Johansson, V., Schroeder, M., Ranius, T., 2016. Local colonization- extinction dynamics of a tree- killing bark beetle during a large- scale outbreak. Ecosphere 7 (3), e01257. http://dx.doi.org/10.1002/ecs2.1257.

Kotsiantis, S.B., Zaharakis, I., Pintelas, P., 2007. Supervised Machine Learning: A Review of Classification Techniques.

Lausch, A., Heurich, M., Gordalla, D., Dobner, H.-J., Gwillym-Margianto, S., Salbach, C., 2013. Forecasting potential bark beetle outbreaks based on spruce forest vitality using hyperspectral remote-sensing techniques at different scales. For. Ecol. Manage. 308, 76–89.

Lausch, A., Erasmi, S., King, D.J., Magdon, P., Heurich, M., 2016. Understanding forest health with remote sensing-part I—A review of spectral traits, processes and remote-sensing characteristics. Remote Sensing 8 (12), 1029.

Lausch, A., Erasmi, S., King, D.J., Magdon, P., Heurich, M., 2017. Understanding forest health with remote sensing-part II—A review of approaches and data models. Remote Sens. 9 (2), 129.

Lehmann, J.R., Nieberding, F., Prinz, T., Knoth, C., 2015. Analysis of unmanned aerial system-based CIR images in forestry—A new perspective to monitor pest infestation levels. Forests 6 (3), 594–612.

Long, J.A., Lawrence, R.L., 2018. Mapping percent tree mortality due to mountain pine beetle damage. For. Sci. 62 (4), 392–402.

Lyytikäinen-Saarenmaa, P., Niemelä, P., Annila, E., 2006. Growth responses and mortality of Scots pine (*Pinus sylvestris* L.). In: Proceedings, Symposium: Forest Insect Population Dynamics and Host Influences. IUFRO Conference, 14–19 September 2003. Kanazawa, Japan. Kanazawa University, Kakuma, Japan. pp. 81–85.

Mäkynen, J., Holmlund, C., Saari, H., Ojala, K., Antila, T., 2011. Unmanned aerial vehicle (UAV) operated megapixel spectral camera. Proc. SPIE 8186. http://dx.doi.org/10.1117/12.897712.

Meddens, A.J., Hicke, J.A., Vierling, L.A., 2011. Evaluating the potential of multispectral imagery to map multiple stages of tree mortality. Remote Sens. Environ. 115 (7), 1632–1642.

Minařík, R., Langhammer, J., 2016. Use of a multispectral uav photogrammetry for detection and tracking of forest disturbance dynamics. ISPRS-International archives of the photogrammetry. Remote Sens. Sp. Inf. Sci. 711–718.

Moriya, E.A.S., Imai, N.N., Tommaselli, A.M.G., Miyoshi, G.T., 2017. Mapping mosaic virus in sugarcane based on hyperspectral images. IEEE J. Sel. Topics Appl. Earth Obs. Remote Sens. 10 (2), 740–748.

Näsi, R., Honkavaara, E., Lyytikäinen-Saarenmaa, P., Blomqvist, M., Litkey, P., Hakala, T., Viljanen, N., Kantola, T., Tanhuanpää, T., Holopainen, M., 2015. Using UAV-based photogrammetry and hyperspectral imaging for mapping bark beetle damage at tree-level. Remote Sens. 7 (11), 15467–15493.

NLS, 2016. National Land Survey of Finland Open Data License. Available online: http://www.maanmittauslaitos.fi/en/opendata/acquisition (Accessed 2 December 2016).

Nevalainen, O., Honkavaara, E., Tuominen, S., Viljanen, N., Hakala, T., Yu, X., Hyyppä, J., Saari, H., Pölönen, I., Imai, N., Tommaselli, A.M., 2017. Individual tree detection and classification with UAV-based photogrammetric point clouds and hyperspectral imaging. Remote Sens. 9 (3), 185.

Oliveira, R.A., Tommaselli, A.M., Honkavaara, E., 2016. Geometric calibration of a hyperspectral frame camera. Photogramm. Rec. 31 (155), 325–347.

Safranyik, L., Carroll, A.L., Régniére, J., Langor, D.W., Riel, W.G., Shore, T.L., Peter, B., Cooke, B.J., Nealis, V.G., Taylor, S.W., 2010. Potential for range expansion of mountain pine beetle into the boreal forest of North America. Can. Entomol. 142 (5), 415–442. http://www.bioone.org/doi/full/10.4039/n08-CPA01.

Senf, C., Seidl, R., Hostert, P., 2017. Remote sensing of forest insect disturbances: current state and future directions. Int. J. Appl. Earth Obs. Geoinf. 60, 49–60.

Siebert, S., Teizer, J., 2014. Mobile 3D mapping for surveying earthwork projects using an Unmanned Aerial Vehicle (UAV) system. Autom. Constr. 41, 1–14.
Smith, G.M., Milton, E.J., 1999. The use of the empirical line method to calibrate remotely sensed data to reflectance. Int. J. Remote Sens. 20, 2653–2662.
Sun, Y., Wong, A.K., Kamel, M.S., 2009. Classification of imbalanced data: a review. Int. J. Pattern Recognit. Artif. Intell. 23 (04), 687–719.
Tanhuanpää, T., Vastaranta, M., Kankare, V., Holopainen, M., Hyyppä, J., Hyyppä, H., Alho, P., Raisio, J., 2014. Mapping of urban roadside trees—A case study in the tree register update process in Helsinki City. Urban For. Urban Green. 13 (3), 562–570.
Torresan, C., Berton, A., Carotenuto, F., Di Genaro, S.F., Gioli, B., Matese, A., Miglietta, F., Vagnoli, C., Zaldei, A., Wallace, L., 2017. Forestry applications of UAVs in Europe: a review. Int. J. Remote Sens. 38 (8–10), 2427–2447.
Tubby, K.V., Webber, J.F., 2010. Pests and diseases threatening urban trees under a changing climate. For.: Int. J. For. Res. 83 (4), 451–459.
White, J.C., Coops, N.C., Wulder, M.A., Vastaranta, M., Hilker, T., Tompalski, P., 2016. Remote sensing technologies for enhancing forest inventories: a review. Can. J. Remote Sens. 42 (5), 619–641.